

Technical Note

Improved Computational Strategies for Rotor Blades Presenting High Gradients in Sectional Properties



Olivier A. Bauchau



Alexander Epple

*Daniel Guggenheim School of Aerospace Engineering
Georgia Institute of Technology
Atlanta, GA*

Sharp gradients in sectional property distributions are inherent to modern rotor blade design and manufacturing practices. The accuracy of finite element models of such rotor blades rapidly degrades if sharp property gradients occur within a single finite element. To remedy this situation, two techniques are developed: first, a mesh optimization procedure based on a measure of local sectional property gradients, and second, a sectional property smoothing technique based on conservation arguments for mass properties and energy considerations for stiffness properties. Numerical experimentation shows that the use of both mesh optimization and sectional property smoothing considerably reduces computational errors in finite element predictions in the presence of property gradients and leads to considerably more monotonic convergence characteristics of the computational process. When the proposed techniques are used, computational requirements are decreased because specified levels of accuracy are achieved for models featuring fewer degrees of freedom; furthermore, better accuracy is obtained when evaluating internal force and moment distributions in the blade.

Nomenclature

d_i	spatial derivatives of sectional properties
E_r	element size ratio
$g(s)$	property gradient index
$h_k(s)$	finite element shape functions
$I_{22}(s)$	flap bending stiffness distribution
k_i	spring constants
ℓ	length of blade
ℓ_i	length of i th finite element
$m(s)$	mass per unit length distribution
N_{el}	number of finite elements
N_{GP}	number of Gauss points per finite element
r	nondimensional variable over a single finite element
s	curvilinear variable along blade axis
s_i	points along blade axis
w_j	weights for Gaussian quadrature
α	relaxation factor
μ	step size of central difference formula

Superscripts

$\overline{(\cdot)}$	smoothed quantity
$(\cdot)'$	derivative with respect to r

*Corresponding author; email: olivier.bauchau@ae.gatech.edu
Manuscript received February 2006; accepted February 2009.

Introduction

For realistic designs, the distribution of rotor blade structural properties presents rapid variations along the blade span. Abrupt changes in mass properties are typically encountered because of the presence of tracking weights used for mass balancing, of various hardware components used in the blade assembly, or of segmented leading edge balance weights. Similarly, steep stiffness variations are not uncommon due to local blade reinforcements such as metal inserts, to various hardware components, or to composite material ply drop-offs. Property variations are often abrupt and typically involve discontinuities of significant magnitude. Both mass and stiffness variations are very pronounced in the root portion of the blade but are also encountered near the tip of the blade, particularly in the presence of swept and tapered blade tips. Finally, rotor blades are often intentionally designed with rapid property variations in an effort to improve dynamic response characteristics through modal shaping.

Some rotorcraft comprehensive analysis codes predict the dynamic response of the blade based on modal reduction techniques (Ref. 1). In this approach, the eigenmodes of the blade are computed first, using a finite element approach, for instance. In view of the rapid variation in sectional properties, a large number of elements are used in the finite element discretization: typically, properties are constant within each element, resulting in high computational costs. However, since modes are computed once only prior to evaluating the dynamic response of the system, this cost remains a very small portion of the total cost of the analysis.

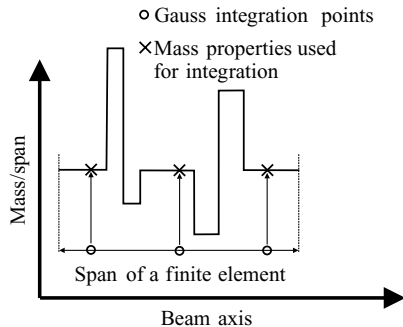


Fig. 1. Evaluation of mass integrals over a typical finite element using Gaussian integration.

In recent years, in an effort to obtain more accurate predictions, some rotorcraft comprehensive analysis codes (Refs. 2–4) have used an alternative approach to the problem: rather than exclusively relying on a modal reduction approach, full finite element representations are maintained throughout the dynamic analysis. Consequently, the cost of the computation becomes directly proportional to the number of elements used in the discretization. If a very fine discretization is required to capture the rapid variations in sectional properties, the cost of the analysis becomes overwhelming.

A potential solution to this problem would be to use coarse finite element meshes. While this approach will reduce computational costs, the accuracy of the analysis might become questionable. In typical finite element formulations, the stiffness and mass matrices of an element are evaluated using Gaussian integration (Ref. 5). Figure 1 shows a hypothetical distribution of mass per unit span over a typical finite element and the locations of the three Gauss points that would be used to evaluate integrals over the element, assuming a four-noded element based on a reduced integration scheme (Ref. 5). For this hypothetical example, the variation in mass properties will be ignored in the integration process: The numerical scheme does not “see” the property variations.

Of course, this problem will disappear with finer meshes, but higher computational costs will result. In this paper, an alternative approach is proposed. First, an optimization technique is developed that automatically generates finite element meshes featuring smaller elements in the area of maximum variation of the physical properties. Second, the original, discontinuous properties are replaced by smeared or averaged properties that enable accurate solutions to be obtained with coarse meshes. The mesh optimization procedure is described in the first section of this paper, whereas the smoothing procedure is described in the next section. Numerical examples illustrating the computational advantages of the proposed procedures are described in the next section. Conclusions are discussed in the last section.

Mesh Optimization Procedure

The purpose of the mesh optimization procedure is to create a finite element mesh of N_{el} elements that reflects sharp changes in its sectional properties. Intuitively, finer meshes, i.e., smaller elements, should be used in an area of sharp property gradients. In addition, it is desirable to refine finite element meshes in areas where the curvature of the undeformed blade changes significantly. The mesh optimization procedure proceeds in two steps. First, a “property gradient index” is defined, and second, an optimum mesh is derived based on this index.

The property gradient index

Let $p_i, i = 1, 2, \dots, n$, be the values of a sectional property, say the blade mass per unit length, or the initial curvature of the blade at equally

spaced points along the blade span, $s_i, i = 1, 2, \dots, n$. The derivation of the property gradient index is based on the evaluation of a smoothed derivative of blade sectional properties. The central difference formula is used to approximate the spatial derivative of the sectional property, d_i , as $d_i = (p_{i+\mu} - p_{i-\mu}) / (s_{i+\mu} - s_{i-\mu})$, where μ indicates the step size of the central difference formula. To further smooth the derivative, the average of derivatives computed with different step sizes is used, leading to

$$d_i = \frac{1}{m} \sum_{j=1}^m \frac{p_{i+\mu_j} - p_{i-\mu_j}}{s_{i+\mu_j} - s_{i-\mu_j}}. \tag{1}$$

Typically, the total number of sampling points was selected as $n = 32N_{el}$, and the following five step sizes ($m = 5$) were used: $\mu_j = 4, 8, 16, 32,$ and 64 . The property gradient index, $g(s)$, is then obtained by averaging the smoothed derivatives computed with the above formula for various sectional properties. The smoothed derivative for each sectional property should be normalized to a unit value to derive the property gradient index.

The spring analogy approach

In the spring analogy, each finite element is associated with a spring of stiffness k_i . The displacement of the last spring is prescribed to be the length of the blade, i.e., $s_{N_{el}} = \ell$. The equilibrium of the system is then obtained from elementary mechanics as

$$\begin{bmatrix} k_1 + k_2 & -k_2 & 0 & & & \\ -k_2 & k_2 + k_3 & -k_3 & & & \\ 0 & & \ddots & \ddots & \ddots & \\ & & & 0 & -k_{N_{el}-1} & k_{N_{el}-1} + k_{N_{el}} \end{bmatrix} \begin{bmatrix} s_1 \\ s_2 \\ \vdots \\ s_{N_{el}-1} \end{bmatrix} = \begin{bmatrix} 0 \\ 0 \\ \vdots \\ \ell k_{N_{el}} \end{bmatrix}, \tag{2}$$

where $s_i, i = 1, 2, \dots, N_{el}$ are the displacements of the points connecting the springs and, by analogy, the location of the finite element nodes; the length of each element is $\ell_i = s_i - s_{i-1}$. Of course, if all spring constants are equal, each spring stretches an equal amount, and by analogy, the sizes of all elements are identical. To optimize the mesh, the stiffness constant is chosen to reflect the local property gradient index

$$\hat{k}_i = \int_{s_{i-1}}^{s_i} g(s) ds \tag{3}$$

It should be noted that the property gradient index, as defined by Eq. (1), could be zero or near zero resulting in a singular system matrix in Eq. (2). Furthermore, since the same force is acting in each spring, the product $\hat{k}_i \ell_i$ must be identical for all elements and hence $\ell_{max} / \ell_{min} = \hat{k}_{max} / \hat{k}_{min}$. In other words, the ratio of the element of maximum size to that of minimum size is equal to the corresponding stiffness constant ratio. In practice, the element size ratio, $E_r = \ell_{max} / \ell_{min}$, is a user-defined value. Hence, the spring constants are scaled as $k_i = \hat{k}_a + \alpha(\hat{k}_i - \hat{k}_a)$, where $\alpha = [(\hat{k}_{max} + \hat{k}_{min})(E_r - 1)] / [(E_r + 1)(\hat{k}_{max} - \hat{k}_{min})]$ and \hat{k}_a is the average value of the spring constants \hat{k}_i . The scaling operation prevents the appearance of zero stiffness constants and results in meshes presenting the desired element size ratio.

The mesh optimization procedure proceeds as follows: Initially, the N_{el} elements are assumed to be of equal length. The spring constants associated with each element are then evaluated, and the equilibrium configuration of the system is found by solving the tridiagonal system defined by Eq. (2) to determine new element nodal locations. The procedure is iterative in nature since the spring constants depend on the element nodal locations. Figure 2 shows a typical property gradient index and the optimum mesh obtained after a few iterations of the spring analogy; the desired element size ratio is $E_r = 4$. A few iterations are required to obtain a converged solution.

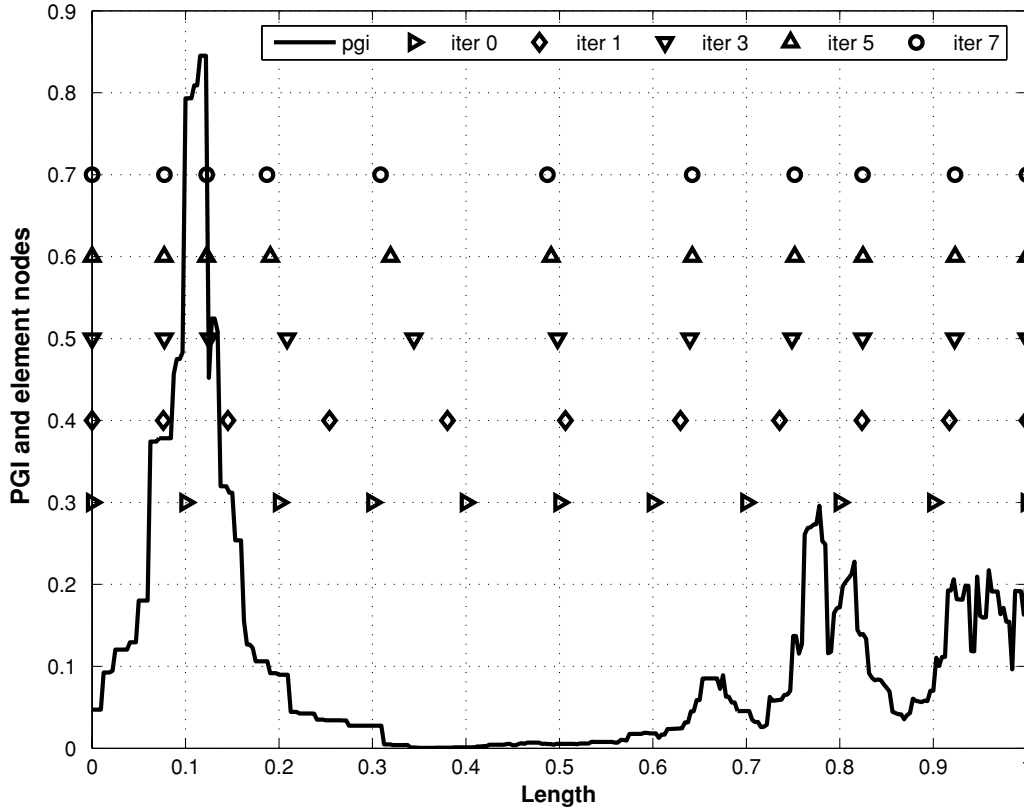


Fig. 2. A typical property gradient index function. Mesh optimization is also illustrated: Starting with 10 equally spaced elements (\triangleright), the four iterations of the spring analogy produce the optimized 10 element mesh (\circ).

Mesh adaptivity

The procedures outlined in the preceding sections can be used as a preprocessing step to a comprehensive analysis. It is also possible to use the same techniques to achieve mesh adaptivity. If the current blade curvature is added to the formulation of the property gradient index, finer meshes will be automatically generated in high deformation areas; the procedure is repeated after a predefined number of time integration steps.

Smoothing Procedure

Consider a curved blade with a curvilinear coordinate s extending from s_0 to $s_{N_{el}}$. For the i th finite element of the blade, a local, nondimensional span variable r is defined such that $r = 2s/\ell_i - (s_i + s_{i-1})/\ell_i$. The location of the Gauss points within this element is given as r_j , $j = 1, 2, \dots, N_{GP}$ (Ref. 5). When evaluating the mass and stiffness matrices of a typical element, the values of the beam's sectional properties are required at the sole Gauss point locations. Hence, it is natural to cast the smoothing procedure in the following terms: Given a finite element mesh, find smoothed sectional properties at the Gauss point locations of all elements.

Mass properties

Consider a blade with an arbitrary "staircase" function describing its mass per unit span distribution, $m(s)$, such as that shown in Fig. 1. The smoothing procedure aims at determining the smoothed mass properties, \bar{m}_j , $j = 1, 2, \dots, N_{GP}$, at the element's Gauss points. To evaluate the

N_{GP} properties, the following equations are proposed:

$$\int_{-1}^{+1} m(r)r^{k-1} dr = \sum_{j=1}^{N_{GP}} w_j \bar{m}_j r_j^{k-1} \quad k = 1, 2, \dots, N_{GP} \quad (4)$$

At first glance, these relationships look like Gaussian quadrature equations that would be written as $\int_{-1}^{+1} m(r)r^{k-1} dr \approx \sum_{j=1}^{N_{GP}} w_j m(r_j)r_j^{k-1}$: the integral on the left-hand side of the equation is *approximated* using Gaussian integration and $m(r_j)$ are the actual values of the mass property at the Gauss points. On the other hand, conditions (4) imply that the left-hand side integrals are *exactly* evaluated by the right-hand side sums when using the smoothed quantities at the Gauss points, \bar{m}_j . The smoothed properties are now readily found by solving the linear system expressed by Eq. (4) to find

$$\begin{bmatrix} w_1 \bar{m}_1 \\ w_2 \bar{m}_2 \\ w_3 \bar{m}_3 \end{bmatrix} = \begin{bmatrix} 1 & 1 & 1 \\ r_1 & r_2 & r_3 \\ r_1^2 & r_2^2 & r_3^2 \end{bmatrix}^{-1} \begin{bmatrix} \int_{-1}^{+1} m(r) dr \\ \int_{-1}^{+1} m(r)r dr \\ \int_{-1}^{+1} m(r)r^2 dr \end{bmatrix} \quad (5)$$

where it was assumed that $N_{GP} = 3$, as an example. The interpretation of these conditions is clear: The smoothed mass properties are such that mass, center of mass location, and moment of inertia of the element, as calculated based on Gaussian quadrature, are identical to the corresponding quantities evaluated based on the detailed property distributions through exact integration. In practice, the integrals on the right-hand side of Eq. (5) are evaluated using Simpson's rule with a very small step size.

Stiffness properties

Next, the procedure is extended to the smoothing of sectional stiffnesses; the flap bending stiffness will be taken as an example. Here again, the goal is to determine smoothed bending stiffnesses, \bar{I}_{22}^j , $j = 1, 2, \dots, N_{GP}$, at the element's Gauss points. The following N_{GP} conditions are proposed:

$$\frac{1}{2} \int_{s_{i-1}}^{s_i} I_{22}(s) \left(\frac{dh_k}{ds} \right)^2 ds = \frac{1}{\ell_i} \int_{-1}^{+1} I_{22}(r) h_k^2(r) dr$$

$$= \frac{1}{\ell_i} \sum_{j=1}^{N_{GP}} w_j \bar{I}_{22}^j h_k^2(r_j) \quad k = 1, 2, \dots, N_{GP} \quad (6)$$

In this expression, the shape functions h_k are selected to be polynomial functions identical to those used in finite element interpolation procedures for elements with N_{GP} nodes. The smoothed properties are now readily found by solving the linear system expressed by Eq. (6) to find

$$\begin{bmatrix} w_1 \bar{I}_{22}^1 \\ w_2 \bar{I}_{22}^2 \\ w_3 \bar{I}_{22}^3 \end{bmatrix} = \begin{bmatrix} h_1^2(r_1) & h_1^2(r_2) & h_1^2(r_3) \\ h_2^2(r_1) & h_2^2(r_2) & h_2^2(r_3) \\ h_3^2(r_1) & h_3^2(r_2) & h_3^2(r_3) \end{bmatrix}^{-1} \begin{bmatrix} \int_{-1}^{+1} I_{22}(r) h_1^2(r) dr \\ \int_{-1}^{+1} I_{22}(r) h_2^2(r) dr \\ \int_{-1}^{+1} I_{22}(r) h_3^2(r) dr \end{bmatrix} \quad (7)$$

The interpretation of these conditions is clear: The smoothed bending stiffnesses are such that strain energy stored in the element, as calculated based on Gaussian quadrature, is identical to that evaluated based on the detailed property distributions through exact integration for specific deformation states of the element characterized by the selected shape functions.

Again, the integrals on the right-hand side of Eq. (7) can be evaluated using Simpson's rule with a small step size. The approach proposed here to smooth flap bending stiffness properties can be applied to other stiffness properties such as axial, torsional, shearing, and bending stiffnesses. Of course, in each case, the procedure must be adapted to evaluate the relevant strain energy, to use appropriate shape functions, and to involve the required number of conditions.

Numerical Results

The approach described in the preceding sections was tested for a simple problem involving a straight, cantilevered rotor blade. The sectional properties of the blade, the mass per unit span, flap and lag bending stiffnesses, and torsional stiffness spanwise distributions are shown in Fig. 3. These properties are representative of typical rotor blade designs. The axial stiffness, flap and lag shearing stiffnesses, and torsional, flap, and lag moments of inertia were computed from the mass per unit span distribution using factors 2.910×10^8 lb-ft/slug, 1.455×10^7 lb-ft/slug, 1.529×10^{-1} ft², 3.820×10^{-2} ft², and 1.147×10^{-1} ft², respectively. These sectional properties will be referred to in the following as the "raw sectional properties."

All numerical simulations presented in this section used a finite element beam model presented by Bauchau (Ref. 6). The shear deformable beam element is based on a geometrically exact formulation and features

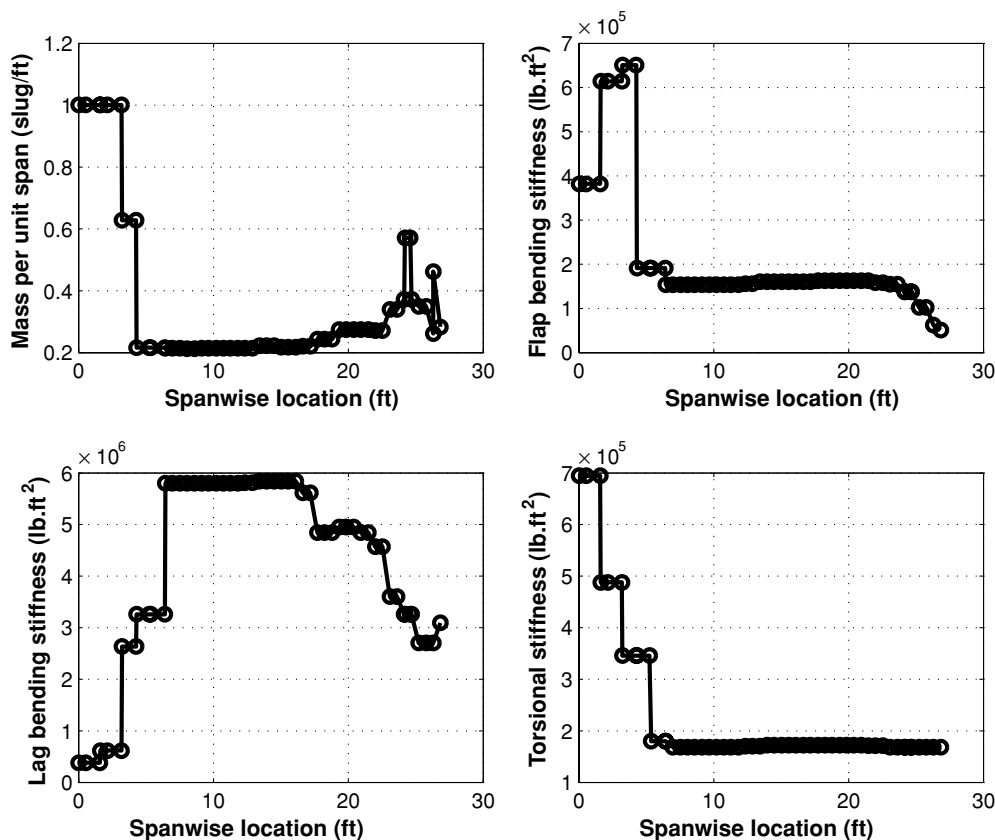


Fig. 3. Property distributions for the blade.

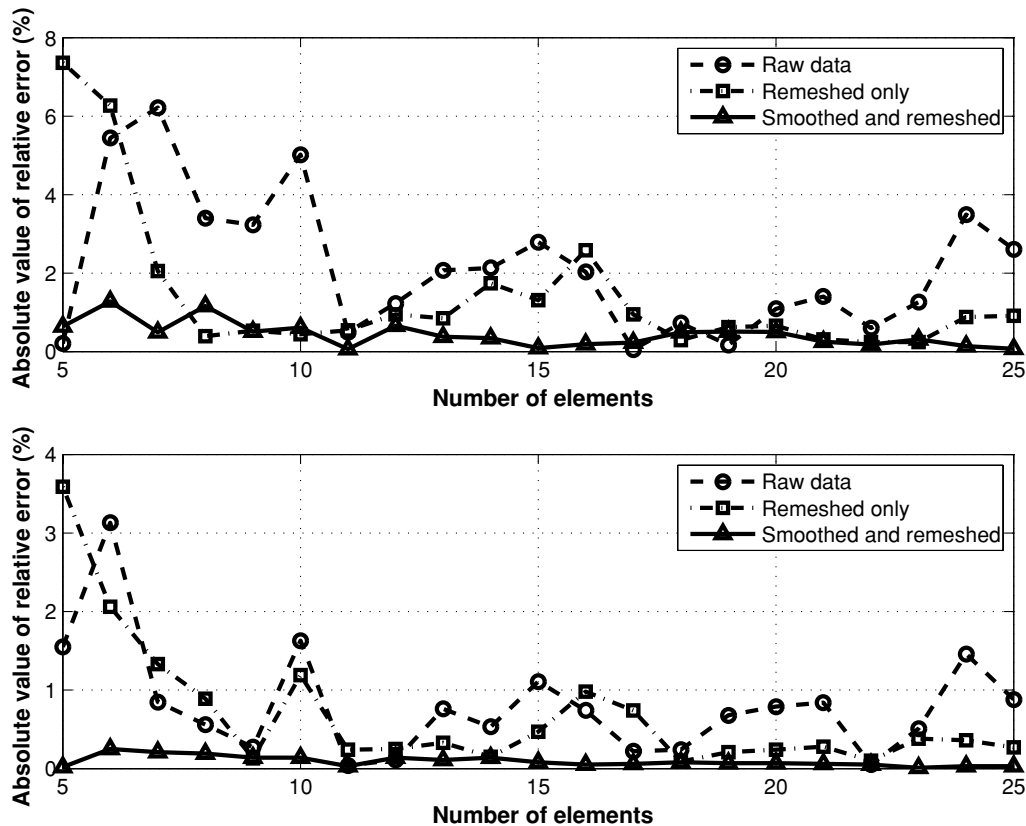


Fig. 4. Comparison of predictions for raw data with equidistant mesh, raw data with optimized mesh, and smoothed data with optimized mesh: first (top graph) and second (bottom graph) lead-lag frequencies.

six degrees of freedom per node, three displacements, and three rotations. In all cases, four noded, cubic elements were used, i.e., cubic polynomials were used to interpolate the displacements and rotation fields. A reference solution of the problem was obtained by using the raw sectional properties and a fine mesh of unequally spaced elements. The raw properties were defined at 54 stations along the span of the blade; 53 cubic elements were used, each spanning a region featuring constant section properties. The convergence of this reference solution was ascertained by running cases where two, three, and four cubic elements were used for each of the regions of constant sectional properties, i.e., for a total of 106, 159, and 212 cubic elements. Identical frequency spectra were obtained for the lowest 12 natural frequencies, demonstrating the convergence of the results.

A series of runs was performed to illustrate the problems encountered by an analyst who wishes to determine an appropriate mesh to study the dynamic response of this blade. The natural frequencies of the blade were computed for meshes featuring an increasing number of equally spaced cubic elements using the raw sectional properties. In each case, absolute values of relative errors in frequencies were computed with respect to the reference solution.

The dashed line in Fig. 4 represents the relative error in the first and second lag frequency as a function of the number of equally spaced elements. Similar results were obtained for flap and torsional frequencies. The very slow convergence of the process is clear: An 8 element mesh produces more than 2% error in the first lag frequency, as do 9, 10, 15, 24, and 25 element meshes. While some meshes produce good results for one or the other frequency, a 24-element mesh is not better than an 8-element mesh despite a threefold increase in the number of degrees of freedom. Since the cost of the analysis is roughly proportional to the number of degrees of freedom, a threefold increase in computational cost has led to no improvement in accuracy. The erratic nature of the conver-

gence illustrated in Fig. 4 is entirely due to the sharp changes in the raw sectional properties. Indeed, it can be proved that for uniform properties, a displacement-based finite element procedure using a consistent mass matrix formulation will produce a monotonic convergence for the natural frequencies of the system (Ref. 5). Before performing extensive comprehensive simulations of rotorcraft systems, it is good engineering practice to determine, through a convergence study, the mesh size that will yield a desired level of accuracy for blade frequencies. A consequence of the nonmonotonic convergence of the predictions is that it becomes very difficult to effectively conduct such a convergence study.

It could be argued that in practice, meshes with *unequally* spaced elements are used to model rotor blades: The analyst will concentrate small elements in regions of rapid property or curvature variations and use larger elements for the remaining portions of the blade, without necessarily using an optimization procedure. At best, this corresponds to the use of raw data with an optimized mesh: The dash-dotted line in Fig. 4 shows the accuracy of the lag frequency predictions to be expected with this approach. While the use of an optimized mesh with raw sectional properties reduces relative errors, the convergence pattern is still unsatisfactory.

Figure 4 also shows the first and second lag frequency predictions obtained by combining the proposed mesh optimization and property smoothing procedures. Similar results were obtained for other frequencies. Clearly, optimizing the mesh and smoothing the properties considerably reduces the absolute value of the relative error; furthermore, the convergence pattern becomes significantly more monotonic. When using the raw sectional data, simply increasing the number of equally or unequally spaced elements does not necessarily yield more accurate results; errors keep increasing and decreasing even when 10, 20 or 25 elements are used.

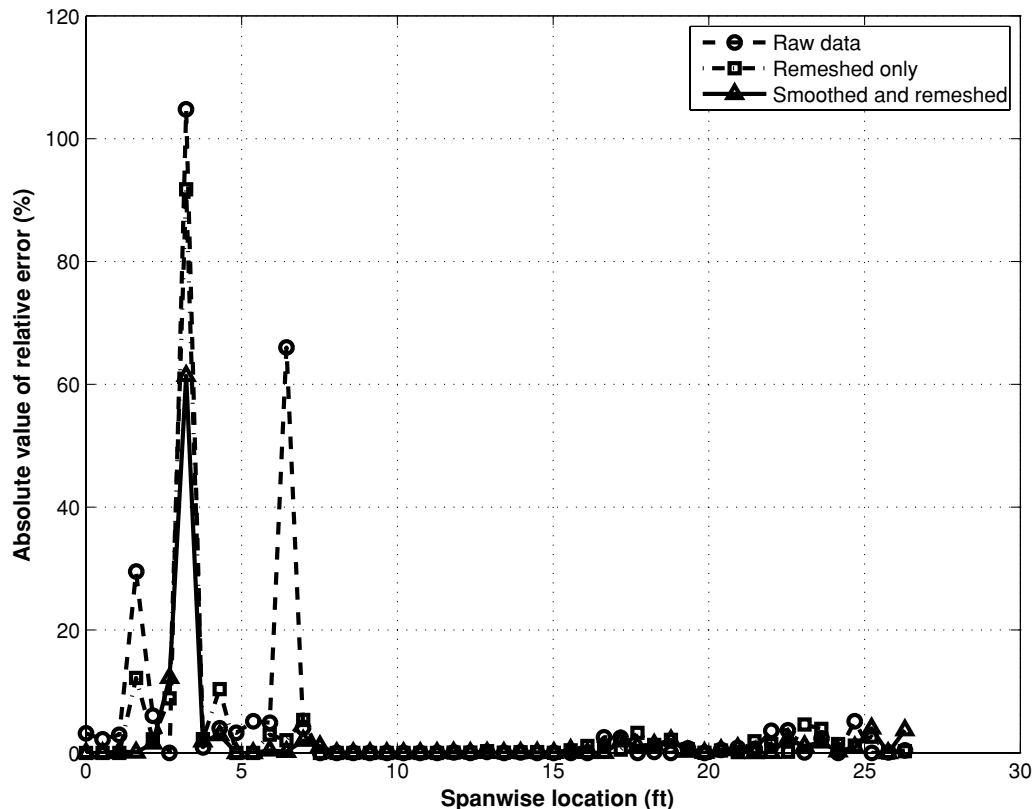


Fig. 5. Comparison of predictions for raw data with equidistant mesh, raw data with optimized mesh, and smoothed data with optimized mesh: lead-lag bending moment.

Finally, the effects of smoothing and mesh optimization on the evaluation of internal forces in the blade were also assessed. Uniformly distributed transverse unit loads were applied to the blade in both flap and lead-lag directions. The exact distribution of flap and lag bending moments were obtained from equilibrium considerations. Next, the same bending moments were computed from the finite element analysis. When using a displacement-based formulation, it is well known (Refs. 7,8) that the Gauss points are superconvergent points for internal stress computations. Hence, the computation of bending moments is a three-step process: First, curvatures are computed at the Gauss points from the nodal rotations and first derivatives of the shape functions; next, Gauss point bending moments are evaluated based on the corresponding curvatures and sectional data; finally, bending moments are extrapolated at any other point within the element based on their Gauss point values.

In many comprehensive rotorcraft codes, internal stresses are computed using the “force summation method,” i.e., based on equilibrium considerations (Ref. 9). In this approach, internal forces are not computed from deformations, and hence sectional properties are not used in the process. Clearly, the force summation method delivers excellent accuracy, even in the presence of sharp variations in sectional properties; however, its application is limited to structures presenting a single load path: For hyperstatic configurations, the equations of equilibrium are not sufficient to evaluate internal forces. It should be mentioned here that one of the reasons for using finite element procedures in rotorcraft comprehensive analysis is to be able to deal with arbitrary configurations, in particular the hyperstatic systems associated with multiple load paths.

The bending moment distributions along the blade were computed using the three-step procedure described above, and predictions were compared to the statics solution for this problem. Figure 5 shows the

absolute value of the relative error for the lag bending moment. Results are shown for a 15 element mesh, using raw data and equally spaced elements in one case, raw data and an optimized mesh in another case, and smoothed properties and an optimized mesh in the third case. Because sectional properties are used in the computation of the bending moment, it is not unexpected that large errors are observed when sharp property gradients occur. The results indicate that the use of raw data and an optimized mesh mitigates these effects to some degree. However, significantly better results can be obtained if smoothed properties and an optimized mesh are used. It should be noted that similar results were obtained for bending in flap direction.

Conclusion

1) Methodologies were presented for optimizing the meshes and smoothing the sectional properties used for the finite element analysis of rotorcraft blades. The mesh optimization procedure is based on a measure of local sectional property gradients. The property smoothing technique is based on conservation arguments for mass properties and energy considerations for stiffness properties.

2) The use of both mesh optimization and sectional property smoothing was shown to considerably reduce computational errors in finite element predictions in the presence of sharp gradients in sectional property distributions.

3) Furthermore, the proposed techniques lead to convergence characteristics that are considerably more monotonic than those observed when using raw sectional data and either equally spaced elements or solely optimized meshes. This allows more meaningful convergence studies to be performed and the determination of mesh configurations that will meet specific error requirements.

4) Computational requirements are considerably decreased when the proposed tools are used because for a specified level of accuracy, significantly less degrees of freedom are necessary.

5) Better accuracy is also obtained for evaluating internal force and moments in the blade when the proposed techniques are used.

References

¹Houbolt, J. C., and Brooks, G. W., "Differential Equations of Motion for Combined Flapwise Bending, Chordwise Bending, and Torsion of Twisted Nonuniform Rotor Blades," NACA Technical Report 1346, 1958. (See also NACA TN-3905, February 1957.)

²Anon., "RCAS Theory Manual, version 2.0," Technical Report USAAMCOM/AFDD TR 02-A-005, U.S. Army Aviation and Missile Command, Moffett Field, CA, June 2003.

³Johnson, W., "Rotorcraft Dynamics Models for a Comprehensive Analysis," American Helicopter Society 54th Annual Forum Proceedings, Washington, DC, May 20–22, 1998.

⁴Bauchau, O. A., Bottasso, C. L., and Nikishkov, Y. G., "Modeling Rotorcraft Dynamics with Finite Element Multibody Procedures," *Mathematical and Computer Modeling*, Vol. 33, 2001, pp. 1113–1137.

⁵Bathe, K. J., *Finite Element Procedures*, Prentice Hall, Inc., Englewood Cliffs, NJ, 1996, Chapters 4 and 5.

⁶Bauchau, O. A., "Computational Schemes for Flexible, Nonlinear Multi-Body Systems," *Multibody System Dynamics*, Vol. 2, 1998, pp. 169–225.

⁷Cook, R. D., Malkus, D. S., and Plesha, M. E., *Concept and Applications of the Finite Elements Method*, John Wiley & Sons, New York, 1989, Chapter 6.

⁸Barlow, J., "Optimal Stress Locations in Finite Element Models," *International Journal for Numerical Methods in Engineering*, Vol. 10, (2), 1976, pp. 243–251.

⁹Bisplinghoff, R. L., Ashley, H., and Halfman, R. L., *Aeroelasticity*, Addison-Wesley Publishing Company, Reading, MA, 1955, Chapter 10.